PAPER • OPEN ACCESS
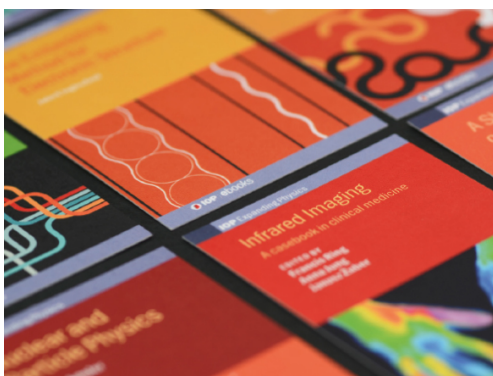
Making copper, silver and gold fullerene cages breathe

To cite this article: W Zhao *et al* 2022 *J. Phys.: Condens. Matter* **34** 224005

View the article online for updates and enhancements.

Making copper, silver and gold fullerene cages breathe

W Zhao[1] , **R M Jones**[1], **R D'Agosta**[2] **and F Baletto**[1,3,*]

[1] Physics Department, King's College London, WC2R 2LS, United Kingdom
[2] Nano-bio Spectroscopy Group, Department of Polymers and Advanced Materials: Physics, Chemistry and Technology, Universidad del País Vasco UPV/EHU, Avenida de Tolosa 72, E-20018 San Sebastián, and Ikerbasque, Basque Foundation for Science, Plaza de Euskadi 5, E-48009 Bilbao, Spain

E-mail: francesca.baletto@unimi.it

CrossMark

Abstract
We show that optical properties change when the fullerene structures of Au_{32}, Cu_{32} and Ag_{32} inflate and deflate. We first observe significant differences in the extinction spectra employing a classical approach based on the Green's dyadic method. By means of real-time time-dependent density functional theory. We continue to calculate the optical spectrum (OP) via a δ-kick simulation, comparing results with the ground-state energetic property the HOMO–LUMO (HL) gap. Red-shift of the OP is expected as the fullerenes inflate, with only $\pm 10\%$ change in the size. As the fullerene breathes, a 0.8 eV shift in the first peak position could be observed in the gold nanoparticle. Ag has a smoother behaviour than both Au and Cu. We have also found changes in the optical spectra can not be directly interpreted as a result of changes in the HL gap.

Keywords: fullerene cage, extinction spectra, optical spectrum, Green's dyadic method, TD-DFT

(Some figures may appear in colour only in the online journal)

1. Introduction

Fullerene cages, i.e., highly symmetric empty structures formed from an icosahedral template, would be ideal building blocks for various applications because of their large surface area, even compared to space-filling structures, and because they may be filled with functional atomic species. Indeed, the inverse of precisely this has already been considered in the literature wherein the optical and magnetic properties of metallic species sequestered within an Si nanosphere has been extensively studied [1–4]. At the same time, we note an increasingly expanding literature reporting optical properties of fullerene cages of different chemical species, among them metallic cages have attracted attention [5–7]. Indeed, gold hollow cages have been recently identified by spectroscopy experiments. The first was the anionic Au_{32}, produced by laser vaporisation of a gold foil, and analysed by photoelectron spectroscopy [8]. Later, smaller anionic Au_{16} and Au_{18}, with a diameter larger than 5.5 Å were stabilised and observed by Bulusu and co-workers [9].

Starting from the first empty icosahedron with 12 atoms, a 'magic' series at 32, 50, 72, 92, and 122 atoms was predicted to be stable, a consequence of both their aromatic character and the $2(k+1)^2$ rule [10]. Wang and co-workers showed that, for structures up to Au_{50}, the aromatic character stabilises the fullerene cage with respect to space-filled isomers [11]. Moreover, they demonstrated that the electronic properties of fullerene cages depend on size, as the HOMO–LUMO (HL) gap approaches a gapless phase for structures containing 92 atoms or more. There is consensus that the tantalising properties of hollow cages are not limited to the icosahedral template.

* Author to whom any correspondence should be addressed.
[3] Also at Physics Department, Universitá di Milano, 20133, Italy; http://balettogroup.org.

Rather, various studies suggest the high-stability of cages between 12 to 30 atoms; either neutral or charged—chiral or achiral [12, 13].

In this study, we focus exclusively on the fullerene cage of 32 atoms. The stability of Au_{32} is remarkable as it satisfies both atomic shell closure, and spherical aromaticity [10, 14]. In our previous study, we found that fullerene Au_{32} shows a high stability, but the same shape represents a (meta)-stable minimum even for copper and silver [15]. As pointed out by Ji *et al*, thermal effects will affect significantly the structures, suggesting that vibrational modes should be considered as well as isomerisation [8]. Furthermore, recent ultra-fast time-resolved optical spectroscopy experiments show two distinct periods for the vibrational modes of ligand-protected metal clusters with a gold core between 0.5–1.5 nm [16]. The slowest mode corresponds to a breathing mode (BM) of the whole cluster. Indeed, it is worth acknowledging the richness of experimental and theoretical contributions to the domain of nanoscience in the pursuit of understanding the interplay between vibrational and optical modes [16–18]. Across these studies, it is generally argued that the collective vibrational eigenmode of uniform radial expansion and contraction, the BM, of finite interacting systems is of great importance as it is profoundly linked to strong correlations within the structure and is widely regarded as one of the fundamental oscillatory characteristics. It has been shown by Henning *et al* that, with only a few extenuating circumstances, many finite systems are prohibited from explicitly exhibiting this particular eigenmode [19]. However; it has conversely been demonstrated that such a mode exists as a quasi-mode for structures within the size range of 0.5–4 nm (13–2057 atoms) [20]. Given that such a fundamental mode may be, *a priori*, assumed to exist, we have elected to explicitly force upon a small cluster this fundamental oscillation, and study how its photo-extinction spectrum may fluctuate throughout the period of oscillation. In particular, we concern ourselves with the consideration of systems undergoing pump–probe spectroscopy experiments, a procedure which is documented to induce the breathing mechanism within samples, to determine whether the induction of this mechanical mode may distort the photo-extinction spectrum of a given sample. In doing so, it is our intention to elucidate upon how the complex interplay between strongly many-body phononic and photonic modes may be seen to affect one another. It has been demonstrated that the typical period for this eigenmode at the considered size is on the order of 1 ps, well within the timeframe for the Landau damping mechanism of localised surface plasmons to occur [21]. Consequently, it may be argued that the effects that this mechanical breathing may have on the plasmonic properties of a given nanoparticle cannot be readily dismissed as trivial and should be considered.

Inspired by experimental observations [16, 20], we investigate how a radial BM might alter the physical properties of the highly symmetric and spherical fullerene cage. We consider both deflation and inflation of the cage. While we expect that different isomers will show different optical spectra, we are solely investigating the effect of small structural changes not altering the shape or the symmetry of the cluster morphology. One can expect that a similar motion might take place

at finite temperatures, further showing the strong coupling between vibration and optical properties in small clusters [18]. Quite surprisingly, we found that even small radial changes affect drastically the electronic and optical properties of noble metal cages. We calculate the optical spectra of fullerene cages of Au, Cu, and Ag at 32 atoms by means of real-time time-dependent density functional theory (RT-TDDFT) and perform comparisons between this *ab initio* TDDFT method and a classical coupled dipole approximation [22]. In doing so, we intend to identify how the quantum mechanical properties of small metallic clusters will result in deviations from a classical electrostatic consideration. We analyse the energetic, electronic, and optical properties of radially inflated and deflated cages, using a dimensionless parameter γ to denote the radial compression/dilatation of up to 12%. While Au and Cu present some similarities, for example, in the main changes between inflated and deflated cages, Ag shows a monotonic red-shift of the first peak of the optical absorption in the visible frequencies. We contrast the change of the position of the first peak in the optical spectra of Au_{32}, Cu_{32}, and Ag_{32} with the HL gap showing that they are not simply related.

This manuscript is organised as follows. In section 2, the theoretical and computational details of the our investigation will be briefly introduced. This includes the fullerene structures used as well as the parameter set of our TDDFT calculation. Section 3 contains our results. A detail analysis of the ground-state properties, and of the optical spectra as a function of the breathing parameters. Finally, we compare the observed changes of the HL and the optical gap.

2. Methodology

The fullerene cages with 32 atoms for pure gold, copper, and silver are shown in figure 1. This cage is obtained removing the inner core of an anti-Mackay icosahedron (Ih) with 42 atoms and it has been shown to be the dual of the most famous C_{60} molecule [24]. We mimic the BM by inflating and deflating the cage in a similar fashion to a little balloon. This is achieved by artificially modifying the average distance of each atom from the centre of mass by radially displacing the atoms by a certain amount. To identify each breathing structure, we introduce a breathing coefficient γ

$$\gamma = \frac{R_{COM}}{R_0} - 1, \qquad (1)$$

where R_{COM} and R_0 represent the average radial distance of the metallic atoms from the centre of mass for the structure, and the ionically relaxed case, respectively. Under this notation, the relaxed stable gold, copper, and silver fullerene correspond to a vanishing breathing coefficient γ. A deflation is identified by a negative breathing coefficient, whereas the inflated shapes have a positive breathing coefficient. We thoroughly examined the structures with γ between -0.09 and 0.12. As we show later by looking at the energetic stability, we do expect that such a BM can take place at finite temperatures. Hence, we can show how relatively small structural changes affect the electronic and optical properties.
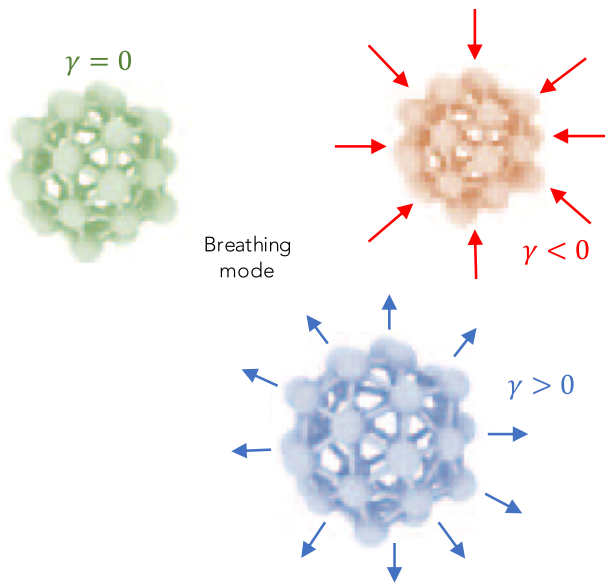
Figure 1. Unperturbed fullerene cage in green, $\gamma = 0$; a deflated cage, with a radial compression and a breathing parameter $\gamma < 0$, is coloured in red, while an inflated cage is in blue ($\gamma > 0.00$, and radial elongation). The figure is obtained through OVITO [23].

For a fast evaluation and screening of the extinction spectrum of the breathing cages, we have also chosen to adopt a classical approach via the Green's dyadic method (GDM) [25, 26], as implemented in the pyGDM code [27, 28]. This method approximates each atom to be a dipole oscillator existing within the coupled dipole approximation. This method neglects explicit electron contributions, hence correlated behaviour that may arise from quantum many-body effects. However, this particular implementation has the benefit of considering the exact position of each atom—respecting the desired geometry of the system while maintaining the relative computational simplicity of a classical approach. An additional advantage of the pyGDM realisation of the GDM method is that, in contrast to most other coupled-dipole codes, pyGDM uses a generalised propagator, which hugely boosts the performance when solving large monochromatic problems. In brief, the GDM seeks to resolve an optical Lippmann–Schwinger equation, calculating the total electromagnetic field inside a nanostructure embedded in a fixed environment. Such systems do not require the presence of an external field, indeed the Lippmann–Schwinger equation self-consistently relates the zero-order field and the total field upon interaction. However, we have elected to illuminate our structures with a series of monochromatic plane waves within the considered spectral range. To evaluate the extinction spectrum, we need only consider the interaction of the dipole moment and total field in each discretised volume cell as,

$$\sigma_{\text{ext}}(\omega) = \frac{8\pi^2}{n_{\text{env}}\lambda_0} \sum_{j}^{N_{\text{cells}}} \Im \left(\mathbf{E}_{0,j}^* \cdot \mathbf{P}_j \right), \qquad (2)$$

wherein n_{env}, λ_0, and $\mathbf{P}_j$ are respectively the dielectric constant of the embedding environment, the incident wavelength, the

dipole moment of cell j, and $E_{0,j} = E_0(r_j)$ is the incident field [29]. In the described method, the near field may be found by self-consistently solving

$$\mathbf{E}(\mathbf{r}_i, \omega) = \mathbf{E}_0(\mathbf{r}_i, \omega) + \sum_{j}^{N_{\text{Cells}}} G_{\text{tot}}^{\text{EE}}(\mathbf{r}_i, \mathbf{r}_j, \omega) \chi \mathbf{E}'(\mathbf{r}_j, \omega) V_{\text{cell}},$$

where $G_{\text{tot}}^{\text{EE}}(\mathbf{r}_i, \mathbf{r}_j, \omega)$ is the Green Dyadic to be solved, χ is the metal's susceptibility, and V_{cell} is the volume of a unit cell. From this field, we then calculate the effective dipole moments, $\mathbf{P}_j = V_{\text{cell}} \chi_j \cdot \mathbf{E}_j$, from the internal field distribution. With knowledge of the functional form of the incident field, and a sufficiently converged internal field distribution, one is able to compute the extinction spectrum for a given finite system held within a dispersive medium, as described by equation (2). All metallic dielectric parameters used in these calculations are provided by Johnson and Christy [30].

A consequence of using known dielectric constants explicitly extracted from systems whose physical size is far greater than that of our own clusters is that it is not unlikely that our systems may begin to appear translucent under illumination. As we are firmly within the quasi-static dipole approximation, by considering structures on the order of 1 nm and illuminating within the UV–vis–NIR (ultraviolet–visible–near-infrared), we may find that the incident field will only weakly couple to the structure and result in non-trivial internal field enhancement as a consequence of this translucency. This is indeed a limitation of the method, and should serve as a stark reminder of the necessity of an *ab initio* method at the nanometric scale. Nonetheless, given the nature of the coupled dipole approximation relying on Coulombic interactions, we may still utilise this method as a fast screening process to search for evidence of novel behaviour—even at such small size scales.

We then accurately calculate the optical properties of breathing hollow cages performing real-time TDDFT calculations, as implemented in *Octopus* [31]. The reason for choosing *Octopus* lies in its real-space and real-time TDDFT computational scheme which is suitable for examining the electronic dynamics of molecular and cluster systems. For both ground state DFT and TD-DFT calculations, a norm-conserving Trouiller–Martins-type fhi88PP pseudo-potential is used. Thus, the exchange and correlation energy is calculated via the PBE-generalised gradient approximation to match the choice of the pseudo-potential [32]. In the real-space TDDFT calculations, the shape and spacing of the spatial grid needs to be set prior to our investigation, and with our early test results, we decide to put each atom inside a vacuum sphere of radius 5.0 Å and we set the spacing at 0.1 Å. These two parameters are carefully selected so that our results are converged within the numerical accuracy of the code. An efficient numerical method of obtaining the absorption spectrum is via the quasi-static dipole approximation. An instantaneous perturbation is applied to the ground state density of the system at time $t_0 = 0$ which takes the form,

$$\mathbf{E}(\mathbf{r}, t) = \mathbf{K}\delta(t) = \frac{1}{\pi} \int_0^{+\infty} d\omega \frac{\hbar\mathbf{k}}{e} \cos(\omega t), \qquad (3)$$

where $\hbar$ and e are the Plank's reduced constant and the electron charge, respectively [33]. It is common to refer to this technique as a 'δ-kick', given that the application of such a perturbation is essentially white light polarised along the vector **k** with incident intensity $|\mathbf{k}|$. Consequently, this perturbation may be considered as a superposition of all frequencies, in which **k** is the electric field's initial polarisation. For the amplitude, we set $|k| = 0.01$ eV Å^{-1} ensuring that any responses to the perturbation are strictly within the linear response regime. After the kick is applied, the system evolves under its own dynamics for a finite, pre-determined period of time. We conclude a given TDDFT simulation by computing the dynamical polarisability $\alpha(\omega)$,

$$\alpha_{pq}(\omega) = \frac{1}{k_q} \int dt \, e^{i\omega t}(d_p(t) - d_p(0)), \qquad (4)$$

where $\mathbf{d}(t) = \int d\mathbf{r} \, n(\mathbf{r}, t)\mathbf{r}$ is the dipole moment calculated from the electron density $n(\mathbf{r}, t)$ [34]. We evaluate the system's strength function, which may be approximated to be the optical extinction spectrum, from the imaginary part of the trace of the polarisability tensor,

$$S(\omega) \propto 2\pi\omega \, \Im\left(\text{Tr}(\alpha(\omega))\right). \qquad (5)$$

As *Octopus* is using a real-time TDDFT scheme in which only the approximate Hamiltonian of one time step further will be calculated through extrapolation of a polynomial fit, it is vital to choose sufficient small time step and a reasonable long total time length to give a numerically-robust spectrum with a sufficiently fine energy resolution to resolve spectral features such as peaks and shoulders. In our simulations, we select a time step of $7 \times 10^{-4}\hbar$ eV $\approx 3 \times 10^{-3}$ fs [35]. Each cluster is evolved for 50 000 time-steps resulting in a total time evolution of approximately 0.15 ps.

3. Results and discussion

First, let us discuss the extinction spectra of breathing fullerene cages, figure 2. We note that the three metals have different behaviour where Au and Cu mainly changing the intensity of their peak well positioned in the visible region. In this respect, Au clusters have just one peak around 2.2 eV, which mildly blue-shift for large and positive γ. However, Cu shows a monotonic change of the intensity as we move from negative to positive values of the breathing parameter. Finally, Ag cages show two clear peaks. The one at higher energies, approximately 3.5 eV, is almost independent from the breathing parameter (its intensity slowly grows with γ), while the one at lower energy shows a dramatic dependence on γ, with a significant blue-shift of its position for inflated cages. It is sufficiently self-evident, even at a classical level as one may observe in figure 2, that during the breathing of a hollow cage we observe changes in the optical properties. However, these variations suffer from the same crude approximations acknowledged in section 2, that is to say that we do not explicitly take into account the interactions between the electrons. With that said, figure 2 demonstrates the necessity in acknowledging the stimulated
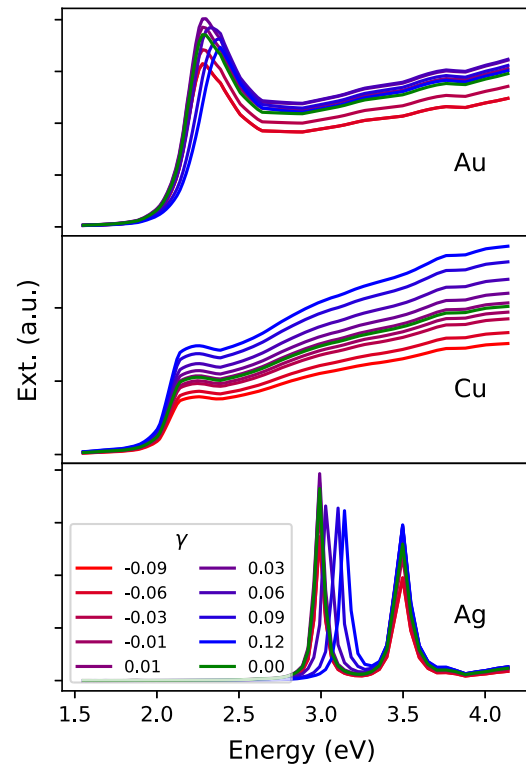
Figure 2. Extinction spectra for Au (top), Cu (middle), and Ag (bottom) fullerene cages, calculated by classical methods through equation (2). Each spectrum computed subject to the illumination of planar waves in the UV–vis–NIR spectral range of 300–800 nm (1.5–4 eV). Figure generated using Matplotlib [36].

variation in extinction spectrum when a nanoparticle is instantaneously illuminated. Moreover, one may appreciate that for larger hollow cage-like structures, the classical spectra displayed in figure 2 will become more representative—though a quantitative investigation of this consideration is beyond the actual scope of this work.

Table 1 reports the ground states energetic properties for the breathing fullerene shape for Au$_{32}$, Cu$_{32}$ and Ag$_{32}$ as a function of the breathing parameter calculated with *Octopus*. We recall that a negative value of the parameter γ stands for a deflation, while a positive value is a inflation. The binding energy per atom, E_B, gives the energy gain with respect to N atoms in the vacuum E^{Vac}

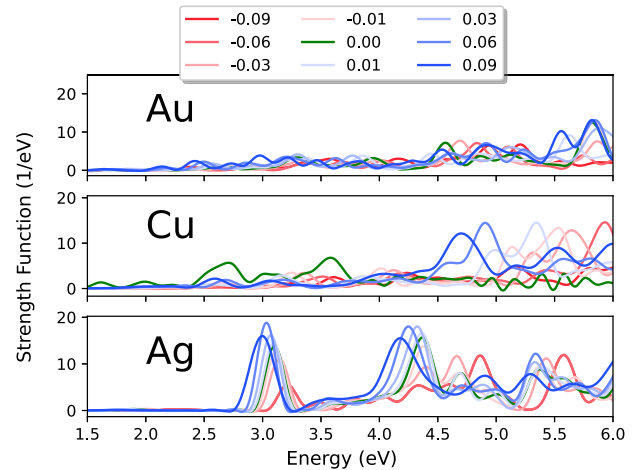$$E_B = \left| \frac{E_{\text{tot}}}{N} - E^{\text{Vac}} \right|, \qquad (6)$$

where E_{tot} is the total energy of the nanosystem. For gold, copper, and silver, the E^{Vac} energies are $E_{\text{Au}}^{\text{Vac}} = -895.9$ eV, $E_{\text{Cu}}^{\text{Vac}} = -1194.9$ eV and $E_{\text{Ag}}^{\text{Vac}} = -982.1$ eV, respectively. Therefore, E_B is an estimate of the stability of each isomer. Being defined as positive, a larger value of E_B implies a more stable configuration. The soft character of copper clusters [37] is evident as radial variations of up to 3% do not alter the binding energy. Similarly, 0.03 eV is the cost for the Au cage to compress by 3%. Conversely, the cost for inflation is slightly higher. Silver is the metal less likely to show radial breathing, with energy cost of at least 40–50 meV for a 1% change of the radius. These considerations led us to the conclusion that

Table 1. Binding energy (E_B), HL gap (E_{HL}), of breathing fullerene of Au_{32}, Cu_{32}, and Ag_{32} for different values of γ, which is an estimate of the average radius against the centre of mass and the average nearest neighbour distance between metallic atoms, d_{NN}.

Element	γ	d_{NN} (Å)	E_B (eV)	E_{HL} (eV)
	−0.09	2.51	2.53	1.65
	−0.06	2.59	2.51	1.59
	−0.03	2.67	2.66	1.56
	−0.01	2.70	2.68	1.54
Au	0.00	2.75	2.69	1.53
	0.01	2.78	2.67	1.52
	0.03	2.84	2.62	1.49
	0.06	2.92	2.51	1.43
	0.09	3.01	2.37	1.31
	0.12	3.09	2.21	1.22
	−0.09	2.21	2.48	0.98
	−0.06	2.28	2.66	1.12
	−0.03	2.35	2.75	1.25
	−0.02	2.37	2.76	1.28
Cu	−0.01	2.40	2.76	1.32
	0.00	2.42	2.76	1.35
	0.01	2.45	2.76	1.39
	0.02	2.47	2.74	1.40
	0.06	2.57	2.65	1.35
	0.09	2.64	2.55	1.31
	−0.06	2.61	1.62	1.21
	−0.03	2.69	1.96	1.47
	−0.02	2.72	1.98	1.51
	−0.01	2.74	1.99	1.54
	0.00	2.77	2.04	1.56
Ag	0.01	2.80	2.00	1.54
	0.02	2.83	1.99	1.51
	0.03	2.86	1.98	1.47
	0.06	2.94	1.93	1.38
	0.09	3.02	1.84	1.29
	0.12	3.11	1.75	1.21

Figure 3. The OP calculated under δ-kick simulation for energy region between 1.5 to 6.0 eV for breathing fullerene Au_{32} (top), Cu_{32} (middle), Ag_{32} (bottom), with breathing coefficient γ varying between −0.09 and +0.09. Figure generated using Matplotlib [36].

the BM could be active when the clusters—especially for the Cu—are kept at a relatively low temperatures.

Figure 3 displays the optical spectra of the fullerene cage of the three noble metals as obtained from the δ-kick in TDDFT. The unperturbed Au cage has a very rough spectra with quite broad and low peaks at 3.3, 3.8, 4.6, 4.8, 5.2, and 5.7 eV. It differs significantly from the one predicted at a classical level. The ionically relaxed Cu-fullerene shows peaks at 1.6, 2.0 eV, a quite broad at 2.75 and 3.6 eV, with a little plateau between them. The 2.75 eV peak is compatible with the peak identified by the GDM approach. Ag seems to show a much clearer optical response and is more consistent with the classical calculations. The fullerene cage has a peak at 3.15 eV and a peak at 4.4 eV, with a shoulder visible already at 4 eV. Three higher energy peaks (between 5.4 and 6 eV) follow. We note that the spectrum of silver cages is well reproduced by the classical tool. The radial motion associated with a BM affects differently the three coinage metals. For gold, there are little changes during the breathing, except for inflation larger than 3%. We might notice a red-shift of the peak at 1.6 eV, during inflation and the appearance of more peaks both in the visible and

the ultraviolet region of the spectrum. Discarding all the features in the strength function below 1.51 eV, which are likely strongly affected by the numerical accuracy of our calculations, the first peak at 3.3 eV would be slightly red-shifted for inflating Au_{32} and blue-shifted up to 3.6 eV for a compression with $\gamma = -0.09$. A stronger effect of the breathing is detectable for the peak at 4.6 eV, with deflation considerably blue-shifting it. On the other hand, inflation causes the appearance of new peaks as for example at 5.55 eV. We should mention photoelectron spectra detect a strong absorption around 4.5–5 eV, and even a stronger peak at 5.5 eV [8]. This might be related to the formation of other isomers, but at the same time it seems compatible with the presence of breathing fullerene cages.

Breathing affects Cu_{32} fullerene in a very peculiar manner. Any distortion seems to flatten its optical response, especially in the visible range. Indeed, distorted copper cages have an almost flat and zero signal up to 2.3 eV. Even mild radial breathing causes a weakening of the peak at 2.75 eV and the appearance of a peak where the ionically relaxed cage has a plateau. The position of this peak blue-shifts from 3.6 to 3.1 eV when changing from $\gamma = -0.09$ to $\gamma = 0.09$. For elongations larger than 6%, we observe the appearance of a higher peak at significant lower energies, around 2.6 eV. On the other hand, the highest peaks are above 4.5 eV. Here, the position of the peaks changes significantly depending on the breathing parameter, with a continuous red-shift of the peak from 5.8 to 4.75 eV when we move from strongly deflated to strongly inflated cages. A silver fullerene cage is the one with the most interesting character, as it shows a clear peak at the border of the visible region (3.1 eV). We note that this peak blue-shifts for radial compression loosing intensity at the same time. The shift of the peak is monotonic from 3.15 to 2.9 eV (or an increase in the wavelength from 387.4 to 427.5 nm, which can be measured). Similarly, we note that the 3.15 eV-peak red-shifts during inflation. A slightly different change can be observed for the second peak at 4.4 eV. Such a peak is affected
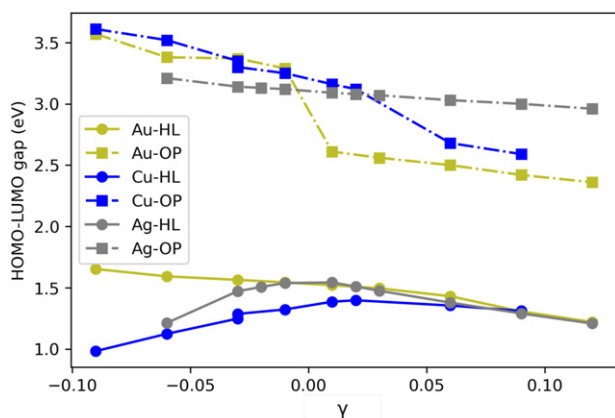
Figure 4. HL gap (full-circles) and OP gap (full-squares) of fullerene cage Au_{32} (in yellow), Cu_{32} (in blue) and Ag_{32} (in grey) as a function of the breathing parameter γ. Figure generated using Matplotlib [36].

by inflation, and again it is red-shifted, but not by deflation. On the other hand strong compression generates 'roughness' of the spectrum between 4.4–5 eV.

The HL gap, E_{HL}, defined as the difference between the highest occupied and the lowest unoccupied molecular orbitals, is reported in table 1. It could be seen that Au_{32} fullerene performs differently than its copper and silver counterparts. As the Au_{32} fullerenes is inflating from smallest radius to the largest, the HL gap is decreasing along the 'inhalation' process in which the hollow space is increasing. Meanwhile, for copper and silver fullerenes, when the structures inflate, the HL gap increase until it reaches a maximum, which are also the most energetically stable structures. Further inflation of the copper and silver fullerene cages induces a reduction of the HL gaps. We note that for any metal and in any case, in correspondence of the value of the HL gap there is no clear absorption peak. Even for the most deflated Au hollow structures which have a larger HL gap, no optical active modes can be detected in the optical spectrum (OP) below 2.0 eV. Generally speaking, one might think that the HL gap could be representative of the optical gap although they pertain to different physical processes [38]. We are going to show that these two quantities poorly correlate during the deflation and inflation.

Figure 4 reports the change of the HL gap obtained from the ground state calculations and the position of the first peak of the OP in the visible region may be obtained from the TDDFT calculations. By considering these two properties with respect to the breathing parameter γ, from -0.09 to 0.12, we may begin to identify strong correlations. Finally, we require that the first peak is defined as the corresponding energy of the first local maximum larger than 1.51 eV. This threshold is carefully chosen so that peaks are clearly detected and reproducible.

We note that the three coinage metals behave very differently, although all show a red-shift for inflated cages (see figure 4). Gold shows an increment of the HL gap while shrinking the cage, and an abrupt blue-shift of the first absorption peak at the transition deflation/inflation. It should be noticed

that the change of HL gap between the smallest deflated gold fullerene and the largest inflated gold fullerene are not comparable with the same difference in the first peak in the OP. On the other hand, copper associates the blue-shift during compression to a reduction of the HL gap. Only the ionically relaxed case shows a peak which can be related with the HL transition. Silver changes monotonically the OP first peak position red-shifting it during inflation. On the other hand, it has a non monotonic variation of the HL gap during inflation and deflation, with a significant reduction (of about 0.4 eV) for compressions/inflations larger than 5%.

Compressed Au and Cu cages display a strong peak above 3 eV, while an expansion yields a peak well within the visible region just above 2.5 eV. The change is abrupt with respect to the equilibrium characteristic inter-atomic radius. Conversely, silver—with the strongest plasmonic character of the coinage metals, due partially to its electrons' high mobility, displays a monotonic blue-shift during the compression of the cage. Furthermore, table 1 demonstrates that the optical gap is strongly negatively correlated with the radius of the nano-cluster. Indeed, this is consistent with what we know of electron–electron interactions. A more compressed structure exhibits electron orbital wavefunctions with strong, non-trivial spatial overlaps and correlations. In promoting the emergence of an excitation through either the collective oscillation of a plasmonic mode or a simple electron–hole creation, one must overcome this correlation with an additional injection of energy. Essentially, this is the ghosts of both Thomas and Fermi reminding us that interacting electrons create a screening effect proportional to their spatial separation. Small noble metal clusters are hence exceptionally good candidates to see the coupling between photon and vibration, and our results show that thermal motion and even simple collective modes can alter significantly their optical properties and the interpretation of future experimental data.

4. Conclusion

Employing RT-TDDFT, we investigate the effect of radial breathing on the electronic and optical properties of fullerene cages of 32 atoms made of gold, copper, and silver. We mimic both an inflation and a deflation of the hollow cage obtained by emptying the core of an anti-Mackay nano-cluster of 42 atoms. We show that a relatively small variation of the radius induces significant changes in both the electronic and the OP of the clusters. Curiously, despite all three candidate metals having a similar electronic profile of a full *d* orbital and a single *s* electron, each set of nanocages exhibited unique behaviour when subject to the mechanical process of breathing. All the considered atomic species and for all the structural distortions show a non-trivial HL gap, in the range 1–1.5 eV. However, Au enlarges its HL gap as a consequences of a radial compression. Ag and Cu have both a non-monotonic behaviour with respect to the breathing parameter. In the copper cages, the radial breathing occurs at a small, if not negligible, energy cost for values of the breathing parameters up to $\pm 3\%$. Its HL gap has a maximum of 1.4 eV when $\gamma = 0.03$.

For Ag cages, the effect is even stronger with changes of about 0.3 eV between the HL for γ of ± 0.09 and the 1.56 eV for the ionically relaxed case at 0 K. Both electrostatic and optical properties appear to behave uniquely when subjected to the mechanical stimulation of a vibrational BM. We then observe a non-trivial relationship between structural changes and optical properties, detected both at the classical and TDDFT level. We note that the GDM approach provides a qualitative and eventually quantitative picture in agreement with TDDFT only for silver. Conversely, gold is poorly reproduced by such a classical framework and requires an atomistic treatment of an *ab intio* method. Generally, an inflation causes a red-shift of the peak position, but the three metals show differences as it occurs. A radial compression of Au flats the optical response below 3.5 eV while an inflation increases the number of peaks in the visible range. The radial motion of Cu cages leads to the disappearance of peaks in the visible region, but well-defined peaks appears in the near-UV. The latter are blue-shifted during deflation. Ag, the metal with a quite strong plasmonic character, shows two clear peaks, both in the extinction and in the absorption spectrum. In the case of relaxed cage the peaks are at 3.1 and 4.4 eV. We note that the former peak red-shift during inflation and blue-shift during deflation. A similar effect follows inflation for the second peak. However, radial compression little changes the position of that peak. We hope that these results may inspire further experimental investigation into the exotic domain of the optical properties of small clusters at finite temperature. In doing so, we anticipate that one may explore the rich physics of coupling between vibrational, optical, and electronic modes.

Acknowledgments

Data availability statement

The data that support the findings of this study will be openly available following an embargo at the following URL/DOI: https://github.com/kcl-tscm/fullerene_breathing.git.

ORCID iDs

W Zhao ⓘ https://orcid.org/0000-0003-3571-3177
R D'Agosta ⓘ https://orcid.org/0000-0002-0173-0705
F Baletto ⓘ https://orcid.org/0000-0003-1650-0010

References

[1] Gueorguiev G K and Pacheco J M 2003 Silicon and metal nanotemplates: size and species dependence of structural and electronic properties *J. Chem. Phys.* **119** 10313–7

[2] Oliveira M J T, Medeiros P V C, Sousa J R F, Nogueira F and Gueorguiev G K 2014 Optical and magnetic excitations of metal-encapsulating Si cages: a systematic study by time-dependent density functional theory *J. Phys. Chem* C **118** 11377–84

[3] Oliveira M I A, Rivelino R, de Brito Mota F and Gueorguiev G K 2014 Optical properties and quasiparticle band gaps of transition-metal atoms encapsulated by silicon cages *J. Phys. Chem* C **118** 5501–9

[4] Pacheco J M, Gueorguiev G K and Martins J L 2002 First-principles study of the possibility of condensed phases of endohedral silicon cage clusters *Phys. Rev.* B **66** 033401

[5] Huang H, Gu G, Yang S, Fu J, Yu P, Wong G K L and Du Y 1998 Third-order nonlinear optical response of fullerenes as a function of the carbon cage size (C_{60} to C_{96}) at 0.532 μm *J. Phys. Chem* B **102** 61–6

[6] Sun Y-P and Riggs J E 1999 Organic and inorganic optical limiting materials from fullerenes to nanoparticles *Int. Rev. Phys. Chem.* **18** 43–90

[7] Paul D, Bhattacharya B, Deb J and Sarkar U 2018 Optical properties of C_{28} fullerene cage: a DFT study *AIP Conf. Proc.* **1953** 030236

[8] Ji M, Gu X, Li X, Gong X, Li J and Wang L-S 2005 Experimental and theoretical investigation of the electronic and geometrical structures of the Au_{32} cluster *Angew. Chem., Int. Ed.* **44** 7119–23

[9] Bulusu S, Li X, Wang L-S and Zeng X C 2006 Evidence of hollow golden cages *Proc. Natl Acad. Sci. USA* **103** 8326–30

[10] Ning H, Wang J, Ma Q-M, Han H-Y and Liu Y 2014 A series of quasi-icosahedral gold fullerene cages: structures and stability *J. Phys. Chem. Solids* **75** 696–9

[11] Wang J, Jellinek J, Zhao J, Chen Z, King R B and von Ragué Schleyer P 2005 Hollow cages versus space-filling structures for medium-sized gold clusters: the spherical aromaticity of the Au_{50} cage *J. Phys. Chem* A **109** 9265–9

[12] Ehlert C, Liu X J and Hamilton I P 2020 Au_{21} cage structures and their magic number tri-cations *Int. J. Quantum Chem.* **120** e26191

[13] Liu X J and Hamilton I P 2017 A series of intrinsically chiral gold nanocage structures *Nanoscale* **9** 10321–6

[14] Wang Q, Halet J-F, Kahlal S, Muñoz-Castro A and Saillard J-Y 2020 Electron count and electronic structure of bare icosahedral Au_{32} and Au_{33} ionic nanoclusters and ligated derivatives. Stable models with intermediate superatomic shell fillings *Phys. Chem. Chem. Phys.* **22** 20751

[15] Baletto F and Ferrando R 2015 Doped golden fullerene cages *Phys. Chem. Chem. Phys.* **17** 28256–61

[16] Maioli P *et al* 2018 Mechanical vibrations of atomically defined metal clusters: from nano- to molecular-size oscillators *Nano Lett.* **18** 6842–9

[17] Crut A, Juvé V, Mongin D, Maioli P, Del Fatti N and Vallée F 2011 Vibrations of spherical core–shell nanoparticles *Phys. Rev.* B **83** 205430

[18] Liu Z, Li Y, Shin W and Jin R 2021 Observation of core phonon in electron–phonon coupling in Au_{25} nanoclusters *J. Phys. Chem. Lett.* **12** 1690–5

[19] Henning C, Fujioka K, Ludwig P, Piel A, Melzer A and Bonitz M 2008 Existence and vanishing of the breathing mode in strongly correlated finite systems *Phys. Rev. Lett.* **101** 045002

[20] Sauceda H E, Mongin D, Maioli P, Crut A, Pellarin M, Del Fatti N, Vallée F and Garzón I L 2012 Vibrational properties of metal nanoparticles: atomistic simulation and comparison with time-resolved investigation *J. Phys. Chem* C **116** 25147–56

[21] Rao V G, Aslam U and Linic S 2019 Chemical requirement for extracting energetic charge carriers from plasmonic metal nanoparticles to perform electron-transfer reactions *J. Am. Chem. Soc.* **141** 643

[22] Ullrich C 2012 *Time Dependent Density Functional Theory: Concepts and Applications* (Oxford: Oxford University Press)

[23] Stukowski A 2010 Visualization and analysis of atomistic simulation data with OVITO-the open visualization tool *Modelling Simul. Mater. Sci. Eng.* **18** 015012

[24] Trombach L, Rampino S, Wang L-S and Schwerdtfeger P 2016 Hollow gold cages and their topological relationship to dual fullerenes *Chem. Eur. J.* **22** 8823–34

[25] Martin O J F, Girard C and Dereux A 1995 Generalized field propagator for electromagnetic scattering and light confinement *Phys. Rev. Lett.* **74** 526–9

[26] Girard C 2005 Near fields in nanostructures *Rep. Prog. Phys.* **68** 1883–933

[27] Girard C 2021 pyGDM (https://pypi.org/project/pyGDM2/)

[28] Wiecha P R 2018 pyGDM-a python toolkit for full-field electrodynamical simulations and evolutionary optimization of nanostructures *Comput. Phys. Commun.* **233** 167–92

[29] Draine B T 1988 The discrete-dipole approximation and its application to interstellar graphite grains *Astrophys. J.* **333** 848

[30] Johnson P B and Christy R W 1972 Optical constants of the noble metals *Phys. Rev.* B **6** 4370–9

[31] Marques M, Castro A, Bertsch G and Rubio A 2003 OCTOPUS: a first-principles tool for excited electron–ion dynamics *Comput. Phys. Commun.* **151** 60–78

[32] Perdew J P, Burke K and Ernzerhof M 1996 Generalized gradient approximation made simple *Phys. Rev. Lett.* **77** 3865

[33] Yabana K and Bertsch G F 1996 Time-dependent local-density approximation in real time *Phys. Rev.* B **54** 4484–7

[34] The roman subscripts refer to the spatial coordinates.

[35] Larger time steps might also lead to numerical instabilities.

[36] Hunter J D 2007 Matplotlib: a 2D graphics environment *Comput. Sci. Eng.* **9** 90–5

[37] Baletto F, Ferrando R, Fortunelli A, Montalenti F and Mottet C 2002 Crossover among structural motifs in transition and noble-metal clusters *J. Chem. Phys.* **116** 3856

[38] Bredas J-L 2014 Mind the gap! *Mater. Horiz.* **1** 17–9